

## Supporting Information

### Figures

# **Synthesis, characterization and adsorption capacity of magnetic carbon composites activated by CO<sub>2</sub>: implication to the catalytic mechanisms of iron salts**

Feng Qian,<sup>1</sup> Xiangdong Zhu,<sup>1,\*</sup> Yuchen Liu,<sup>1</sup> Shilai Hao,<sup>1</sup> Zhiyong Jason Ren,<sup>2</sup> Bin Gao,<sup>3</sup>

Ruilong Zong,<sup>4</sup> Shicheng Zhang,<sup>1,\*</sup> Jianmin Chen<sup>1</sup>

<sup>1</sup> Shanghai Key Laboratory of Atmospheric Particle Pollution and Prevention (LAP3), Department of Environmental Science and Engineering, Fudan University, Shanghai 200433, China

<sup>2</sup> Department of Civil, Environmental, and Architectural Engineering, University of Colorado Boulder, Boulder, CO 80309, United States

<sup>3</sup> Department of Agricultural and Biological Engineering, University of Florida, Gainesville, Florida 32611, United States

<sup>4</sup> Department of Chemistry, Tsinghua University, Beijing 100084, China

\* Corresponding author, Tel/fax: +86-21-65642297; E-mail: [zxdjewett@fudan.edu.cn](mailto:zxdjewett@fudan.edu.cn) (Xiangdong Zhu), [zhangsc@fudan.edu.cn](mailto:zhangsc@fudan.edu.cn) (Shicheng Zhang).

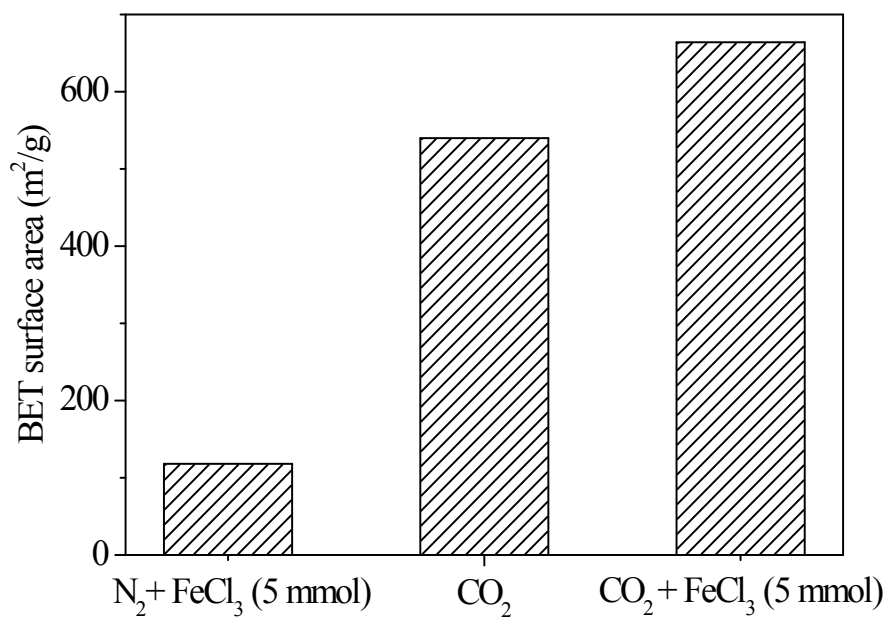


**Fig. S1** Effect of FeCl<sub>3</sub> and CO<sub>2</sub> gas on the porosity of as-prepared MCs (750°C of activation temperature and 2 h of hold time).

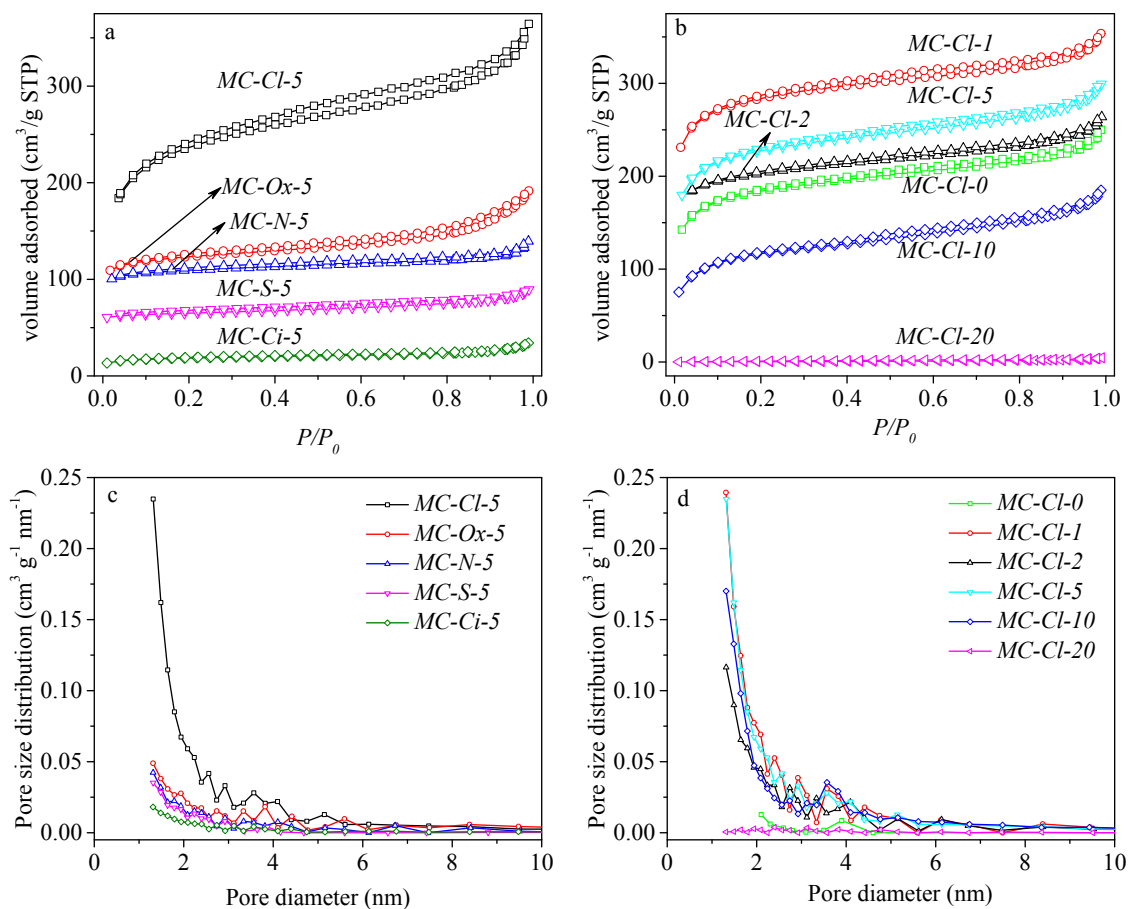


**Fig. S2** (a) N<sub>2</sub> adsorption-desorption isotherms for different iron salt type derived MCs, (b) N<sub>2</sub> adsorption-desorption isotherms for different FeCl<sub>3</sub> loading content derived MCs, (c) pore size distributions for different iron salt type derived MCs, (d) pore size distributions for different iron FeCl<sub>3</sub> loading content derived MCs (750°C of activation temperature and 2 h of hold time).

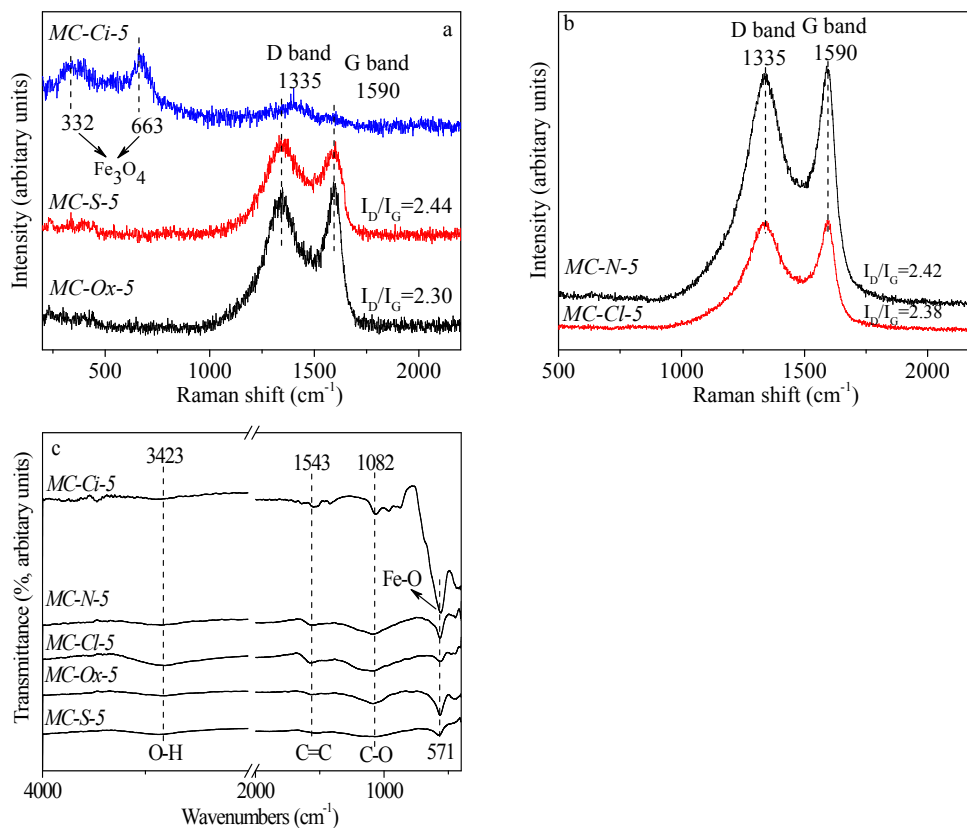


**Fig. S3** (a, b) Effect of iron salt types on the Raman spectra of the resulting MCs, (c) effect of iron salt types on the FTIR spectra of the resulting MCs (750°C of activation temperature and 2 h of hold time).

**Note:** The Raman spectrum of *MC-Ci-5* showed two intense peaks at around 332  $\text{cm}^{-1}$  and 663  $\text{cm}^{-1}$ , which were attributed to be  $E_g$  and  $A_{1g}$  vibrational modes of the  $\text{Fe}_3\text{O}_4$  phase (Fig. S3a and S3b). The disappearance of the D band (1335  $\text{cm}^{-1}$ ) and G band (1590  $\text{cm}^{-1}$ ) confirmed the over-activation of the *MC-Ci-5* sample, which was further validated by the strong Fe-O stretching (571  $\text{cm}^{-1}$ ) in the FTIR spectrum of the *MC-Ci-5* sample (Fig. S3c).

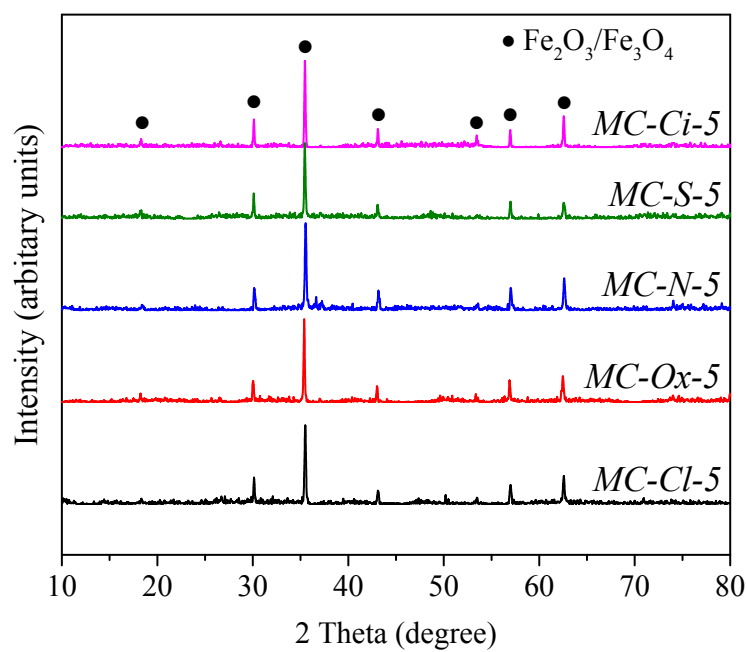


**Fig. S4** Effect of iron salt types on the XRD patterns of resulting MCs (750°C of activation temperature and 2 h of hold time).

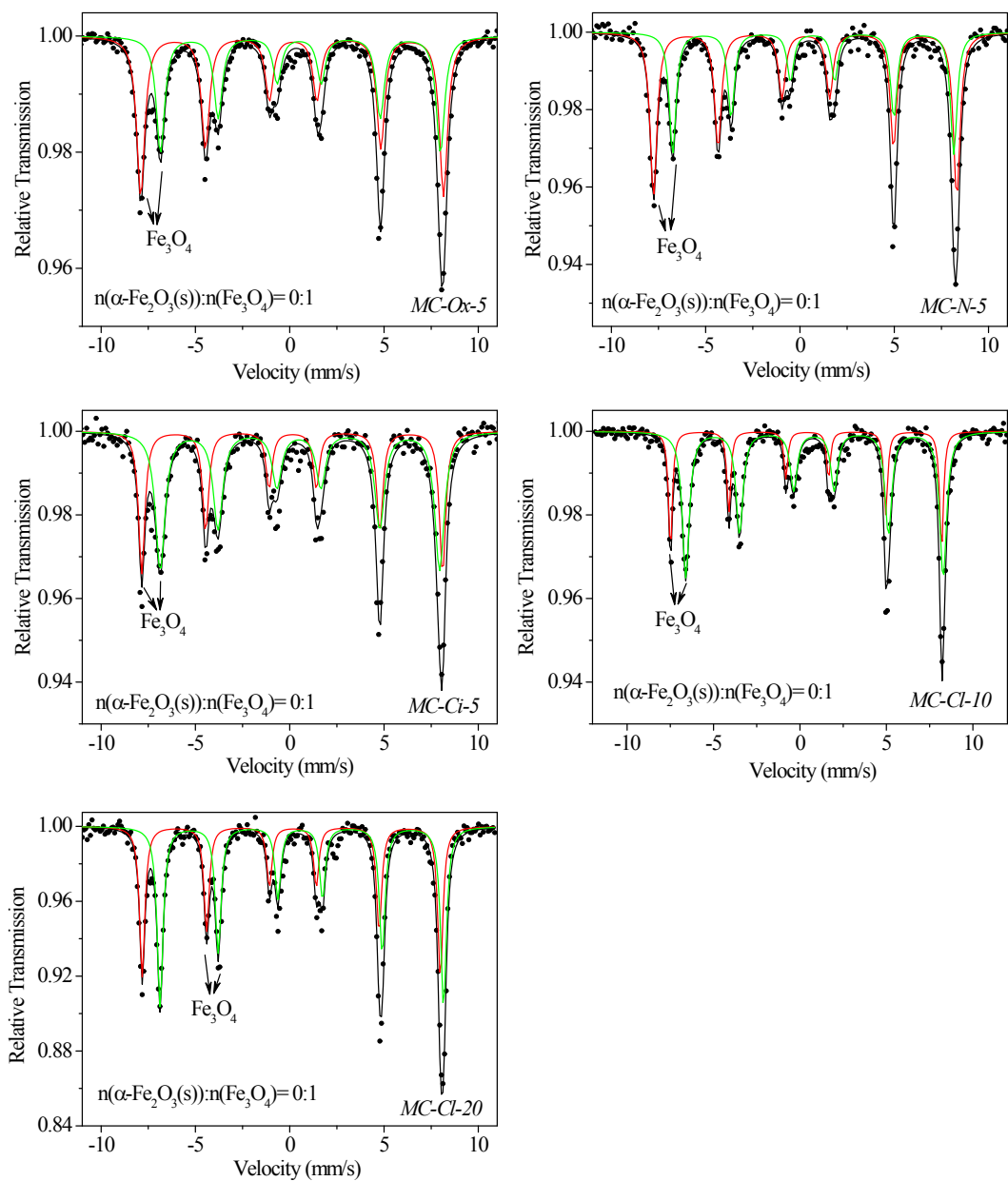


**Fig. S5** Room-temperature Mössbauer spectra of selected MCs (750°C of activation temperature and 2 h of hold time).

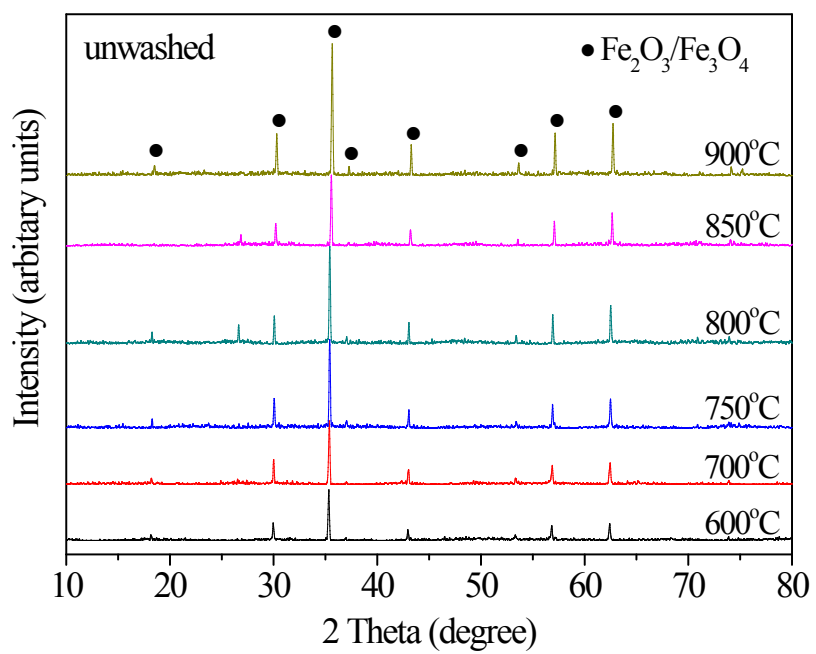


**Fig. S6** Effect of activation temperature on the XRD patterns of unwashed MCs (MCs were fabricated by 5 mmol of FeCl<sub>3</sub> for 2 h).

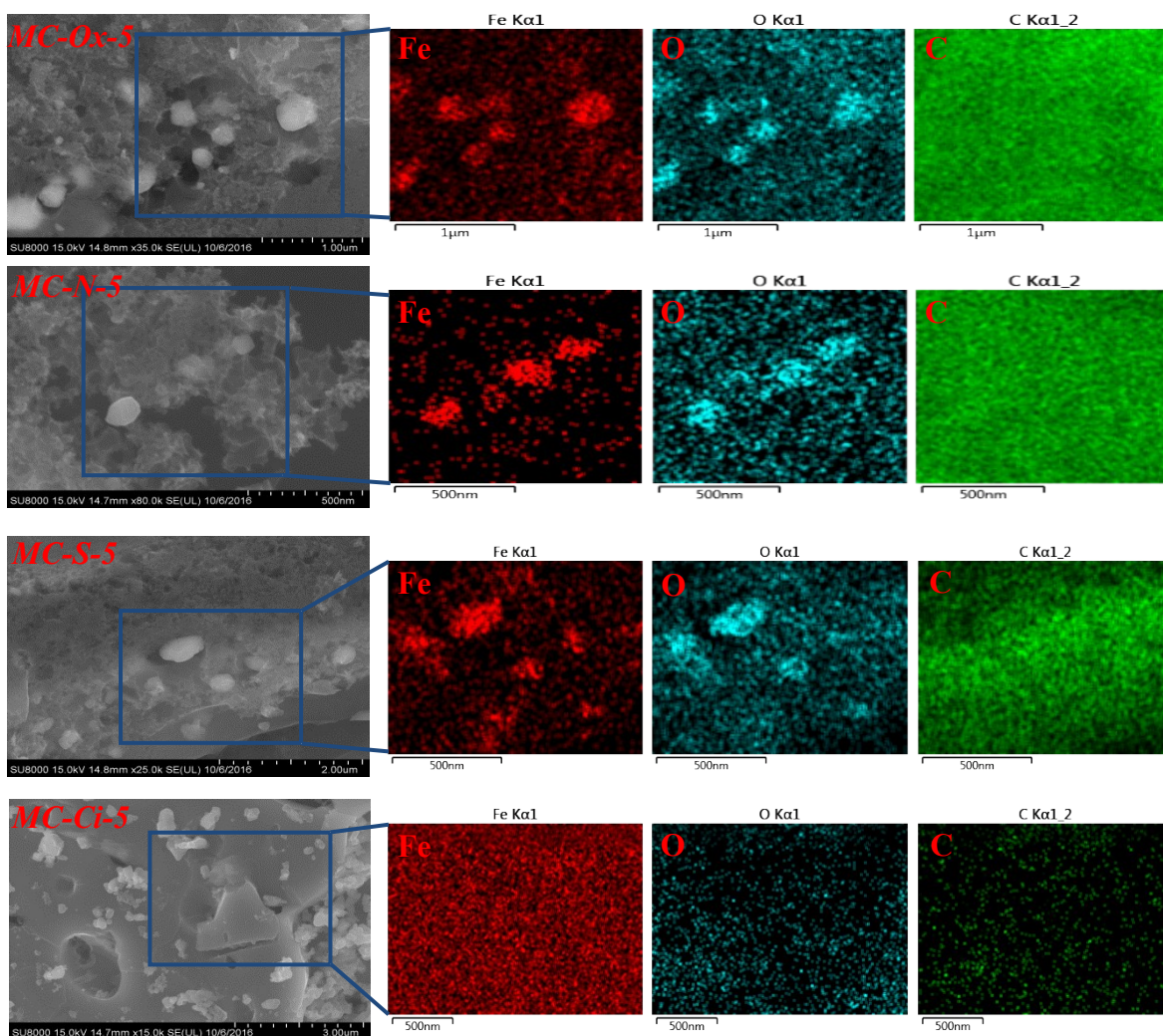


**Fig. S7** SEM images and elemental mapping (Fe, O and C) images of different iron salts derived MCs.



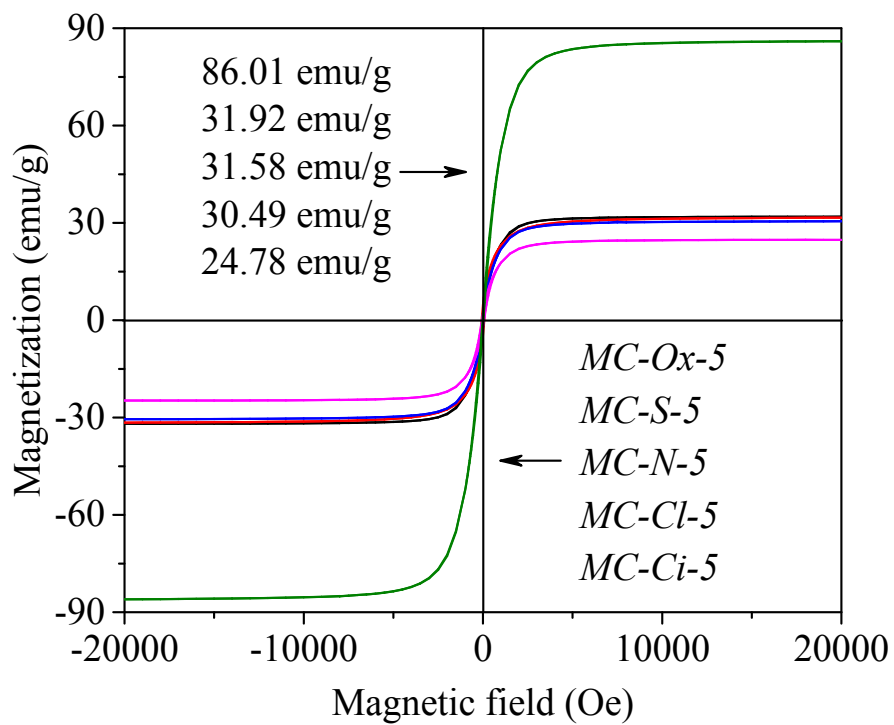


**Fig. S8** The hysteresis loops of the MCs derived from different iron salt types under 25°C (750°C of activation temperature and 2 h of hold time).

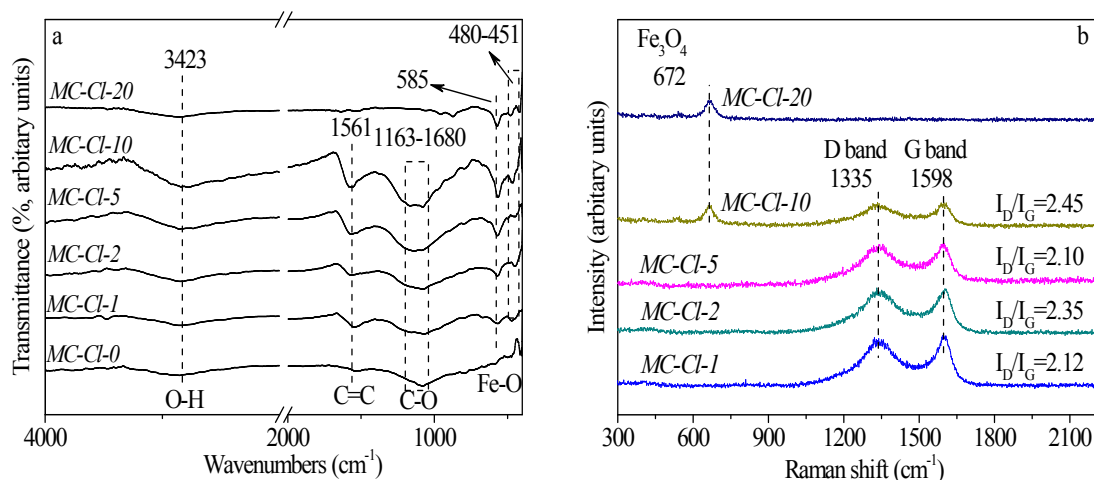


**Fig. S9** (a) Effect of FeCl<sub>3</sub> content on the FTIR spectra of the resulting MCs and (b) effect of FeCl<sub>3</sub> content on the Raman spectra of the resulting MCs (750°C of activation temperature and 2 h of hold time).

**Note:** As shown in Fig. S9a, the C=C stretching in aromatic groups and C-O vibration (~ 1561 cm<sup>-1</sup> and 1163-1180 cm<sup>-1</sup>) disappeared in *MC-Cl-20* sample. However, Fe-O stretching in Fe<sub>3</sub>O<sub>4</sub> (585 cm<sup>-1</sup> and 480-451 cm<sup>-1</sup>) became stronger, indicating that less carbon matrix was retained in the *MC-Cl-20* sample. Likewise, the Raman spectrum of *MC-Cl-20* sample was dominated by the Fe<sub>3</sub>O<sub>4</sub> signal (Fig. S9b). The FTIR and Raman spectra further confirmed the evolution of reaction between carbon matrix and CO<sub>2</sub> gas, influenced by the FeCl<sub>3</sub> content.

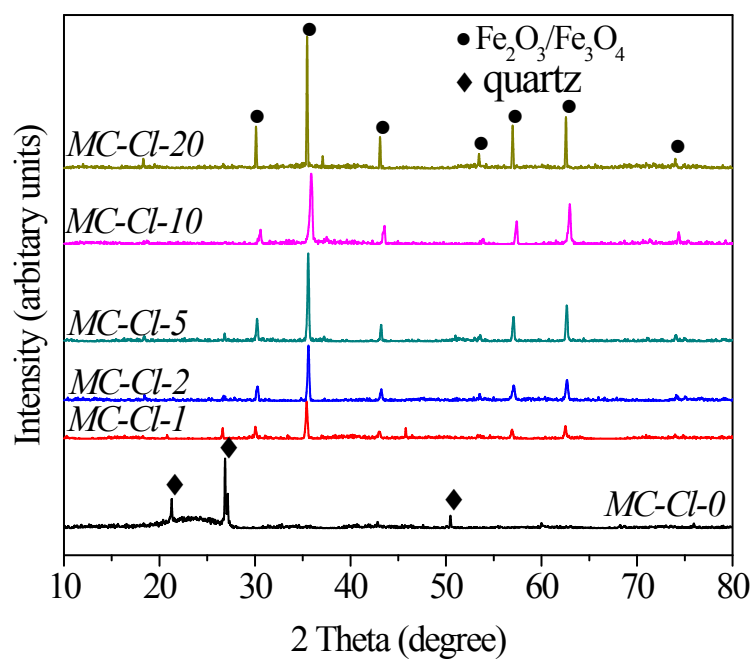


**Fig. S10** Effect of FeCl<sub>3</sub> loading content on the XRD patterns of resulting MCs.

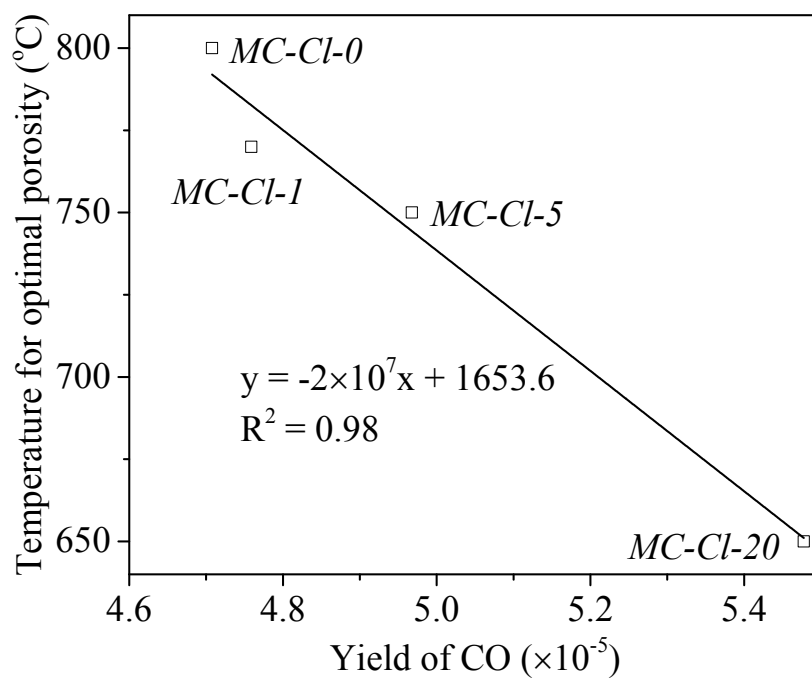


**Fig. S11** Correlation between of the yield of CO (integral area of CO release curve) and temperature for optimal porosity of MCs derived from different  $\text{FeCl}_3$  loading content.

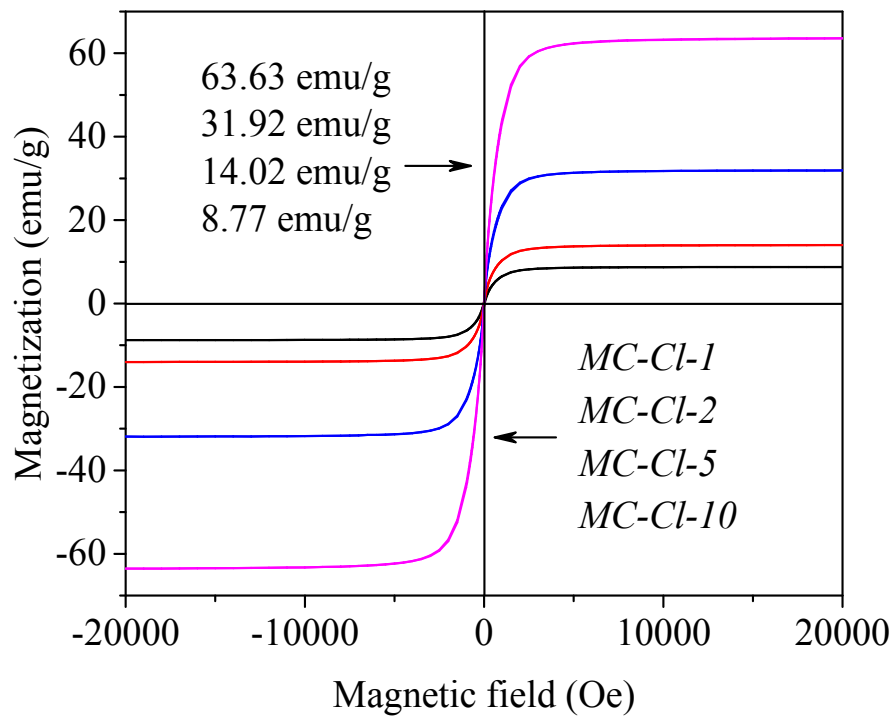


**Fig. S12** The hysteresis loops of the MCs derived from different FeCl<sub>3</sub> loading content under 25°C (750°C of activation temperature and 2 h of hold time).

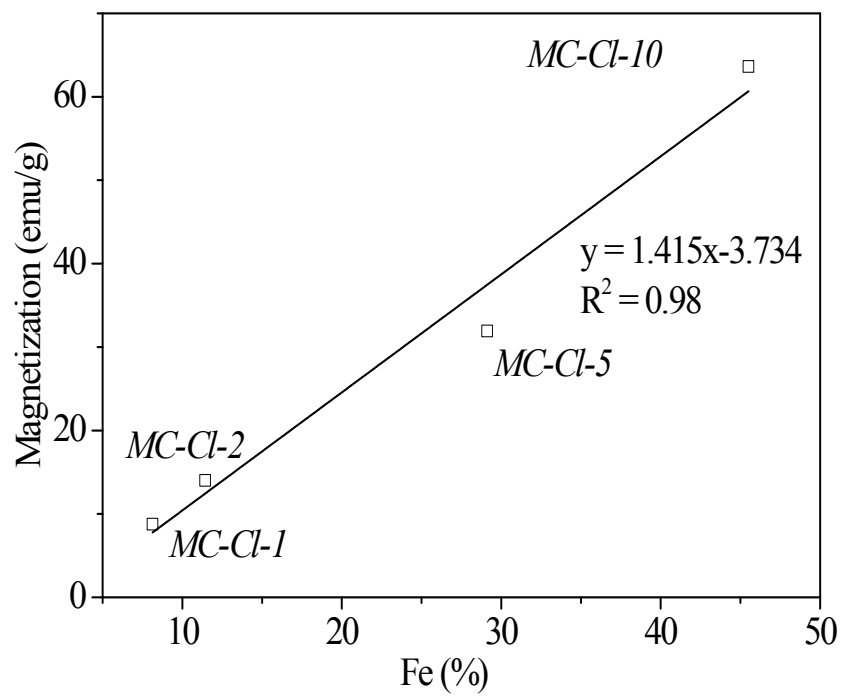


**Fig. S13** Correlations between Fe content (%) and magnetization of different FeCl<sub>3</sub> loading content derived MCs samples.

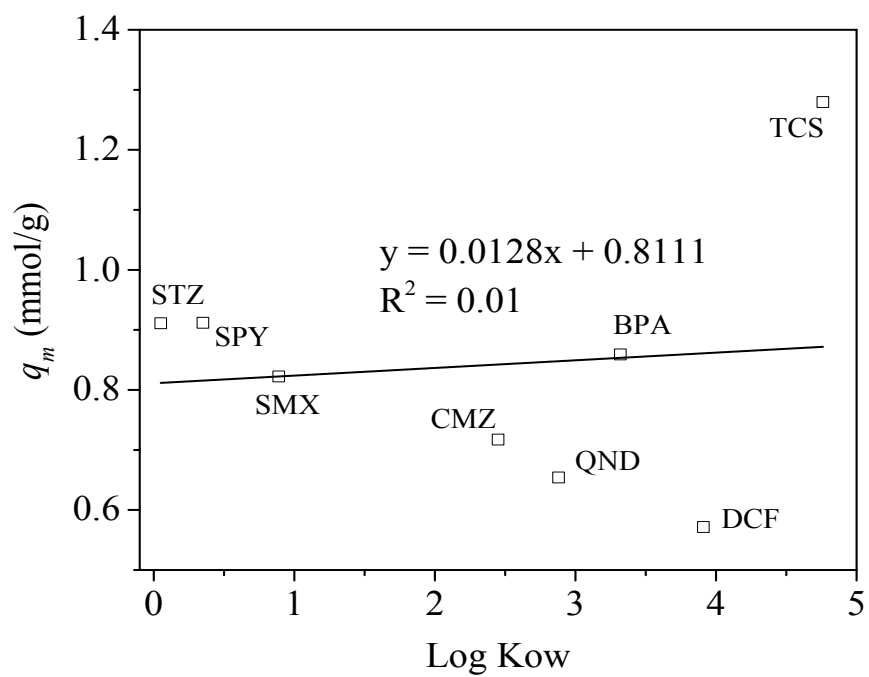


**Fig. S14** A linear relationship between  $\text{Log } K_{OW}$  and  $q_m$  of PPCPs on *MC-CI-5* sample.